AD-A191 324 THOMSON SCATTERING FOR DETERMINING ELECTRON CONCENTRATIONS AND TEMPERATUR (U) INDIANA UNIV AT BLOOMINGTON DEPT OF CHEMISTRY K A MARSHALL ET AL 1/1

UNCLASSIFIED 15 FEB 88 INDU/DC/GMH/TR-88-19 F/G 20/9 NL

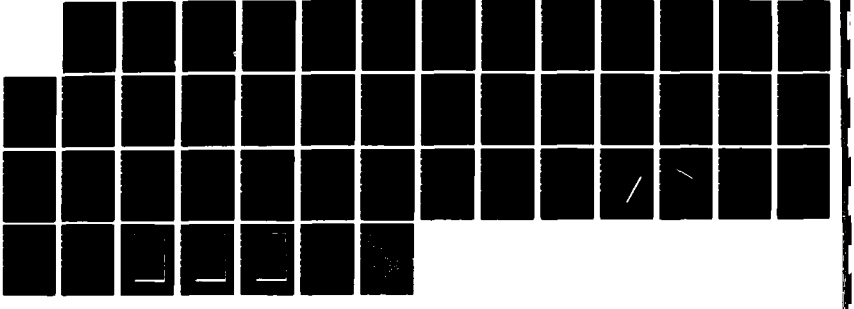

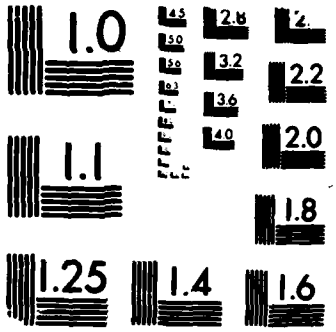

UNCLASSIFIED

SECURITY CLASSIFICATION OF THIS PAGE

DTIC FILE COPY

4

REPORT DOCUMENTATION PAGE

AD-A191 324

1b. RESTRICTIVE MARKINGS
NA

3. DISTRIBUTION/AVAILABILITY OF REPORT
Distribution Unlimited; Approved for Public Release

2b DECLASSIFICATION/DOWNGRADING SCHEDULE
NA

4 PERFORMING ORGANIZATION REPORT NUMBER(S)
INDU/DC/GMH/TR-88-19

5. MONITORING ORGANIZATION REPORT NUMBER(S)
NA

6a. NAME OF PERFORMING ORGANIZATION
Indiana University

6b. OFFICE SYMBOL (If applicable)
NA

7a. NAME OF MONITORING ORGANIZATION
ONR

6c. ADDRESS (City, State, and ZIP Code)
Department of Chemistry
Bloomington, IN 47405

7b. ADDRESS (City, State, and ZIP Code)
800 N. Quincy Street
Arlington, VA 22217

8a. NAME OF FUNDING/SPONSORING ORGANIZATION

8b. OFFICE SYMBOL (If applicable)

9 PROCUREMENT INSTRUMENT IDENTIFICATION NUMBER
Contract N00014-86-K-0366

8c. ADDRESS (City, State, and ZIP Code)

10 SOURCE OF FUNDING NUMBERS

PROGRAM ELEMENT NO.	PROJECT NO.	TASK NO	WORK UNIT ACCESSION NO
		R&T Code 4134006	

11 TITLE (Include Security Classification) Thomson Scattering for Determining Electron Concentrations and Temperatures in an Inductively Coupled Plasma. II. Description and Evaluation of a Multichannel Instrument.

12 PERSONAL AUTHOR(S)
Kim A. Marshall and Gary M. Hieftje

13a TYPE OF REPORT	13b TIME COVERED	14. DATE OF REPORT (Year, Month, Day)	15 PAGE COUNT
Technical	FROM _____ TO _____	15 February 1988	44

16 SUPPLEMENTARY NOTATION
Accepted for publication in Spectrochimica Acta

17 COSATI CODES		
FIELD	GROUP	SUB-GROUP

18. SUBJECT TERMS (Continue on reverse if necessary and identify by block number)
Thomson scattering; Inductively coupled plasma; Multielement analysis.

19 ABSTRACT (Continue on reverse if necessary and identify by block number)

A new instrument has been assembled to measure Thomson scattering from an inductively coupled plasma. Unlike previous designs, the new system employs a fiber-optic array to measure simultaneously up to 12 channels on a Thomson-scattering spectrum. Shutters enable either side of the nominally symmetrical Thomson spectrum to be examined, or permit summing equally spaced channels on opposite sides of the spectrum from the incident laser wavelength. A central channel, used to monitor Rayleigh scattering, enables a simultaneous determination of true gas-kinetic temperatures. Photodetector fatigue is avoided through a rotating mirror that serves as an optical shutter while individual gated integrators attached to each detector minimize the detection of background radiation from the plasma. The new instrument offers high stray-light rejection capability and provides measurements whose precision is photon-limited. Results obtained with the new instrument are presented in a companion paper.

20 DISTRIBUTION/AVAILABILITY OF ABSTRACT
☒ UNCLASSIFIED/UNLIMITED ☐ SAME AS RPT ☐ DTIC USERS

21 ABSTRACT SECURITY CLASSIFICATION
Distribution Unlimited

22a NAME OF RESPONSIBLE INDIVIDUAL
Gary M. Hieftje

22b. TELEPHONE (Include Area Code)
(812) 335-2189

22c. OFFICE SYMBOL

DTIC ELECTE FEB 25 1988 S

DD FORM 1473, 84 MAR

83 APR edition may be used until exhausted
All other editions are obsolete

SECURITY CLASSIFICATION OF THIS PAGE

UNCLASSIFIED

OFFICE OF NAVAL RESEARCH

Contract N14-86-K-0366

R&T Code 4134006

TECHNICAL REPORT NO. 19

THOMSON SCATTERING FOR DETERMINING ELECTRON CONCENTRATIONS AND TEMPERATURES IN AN INDUCTIVELY COUPLED PLASMA

II. DESCRIPTION AND EVALUATION OF A MULTICHANNEL INSTRUMENT

by

K. A. Marshall and G. M. Hieftje

Prepared for Publication

in

SPECTROCHIMICA ACTA

Indiana University
Department of Chemistry
Bloomington, Indiana 47405

15 February 1988

1. INTRODUCTION

Thomson scattering has been shown to be capable of measuring, on a spatially and temporally resolved basis, both electron concentrations and temperatures in plasmas of various kinds [1,2]. In a companion paper [3], we reveal how a new multichannel instrument for performing Thomson-scattering measurements can help unravel the many and complex processes that occur in the analytical inductively coupled plasma (ICP). Here, we will outline in detail the considerations that led to the development of the multichannel system, describe its design and construction, and assess its performance.

The new instrument was designed when the shortcomings of an earlier single-channel system [4,5] were realized. This earlier unit was proven capable of minimizing stray-light problems and of producing usable Thomson-scattering spectra. However, the use of a relatively low repetition-rate laser source required data-collection times that were excessively long. During the long periods required for acquisition of a single Thomson spectrum, ICP drift occurred and rendered the resulting data interpretation suspect. As a consequence, values for both electron number density (concentration) and temperature could be considered only approximate.

The new instrument to be described here alleviates these difficulties. It possesses a multichannel read-out system so a complete Thomson-scattering spectrum can be acquired at once. Also, photodetector fatigue is overcome through use of a rotating-mirrored chopper which permits each detector in the multichannel array to view the ICP for only the brief period during which the Thomson signal is generated. Finally, a bank of gated integrators samples the signals from individual photodetectors for just that time when the detectors are receiving Thomson-scattered light.

At the heart of the new device is a fiber-optic array placed at the focal plane of the Thomson spectrometer. Specially fabricated for this application, the array simultaneously collects radiation from 25 discrete wavelengths across the Thomson spectrum and carries the light to a group of 13 individual photomultipliers. One of the detectors views the incident laser wavelength and thus records Rayleigh scattering; the other 12 channels register one half of a Thomson spectrum. Through manipulation of a set of shutters incorporated into the photodector housing, one can elect to monitor either side (red- or blue-shifted) of the spectrum, or to fold the two halves in order to increase signal-to-noise ratios.

The new instrument is found to have stray-light rejection capabilities similar to its single-channel counterpart. Also, the ability to acquire Thomson spectra rapidly makes the new device much less susceptible to drift in the electronic, optical, or plasma components. However, greatest uncertainty in a scattering spectrum occurs in the wings, where the influence on electron temperatures is greatest. Consequently, values for electron temperature are still less reliable than is desired, although electron-concentration measurements are judged to be acceptable. Precision in the wings of the Thomson spectrum appears to be limited by photon statistics.

2. EXPERIMENTAL

2.1 Similarities with the Single-channel Instrument

A block diagram of the multi-channel instrument is shown in Fig. 1. This figure helps clarify the interrelationship of the many components of this scattering system, and displays the 135° scattering geometry. The instrumental geometry and many hardware portions of the

system are similar or identical to those of the single-channel arrangement [4,5]. Specifically, the scattering geometry, the Q-switched ruby laser, focusing optics and beam stops, the beam dumps, viewing dump and torchbox construction are the same as earlier. Details on this system can be found elsewhere [4]; however, a brief review is warranted here.

A Q-switched ruby laser (model K1 laser head and model KQS2 Q-switch, Korad Division of Hadron, Inc., Santa Monica, CA) with an output power of approximately 20 MW (0.5 joules/pulse) provides the incident 25-ns light pulse at 694.3 nm. A vertical laser polarization was selected to maximize the scattering signal. The laser beam is focused by a two-lens optical system. The first lens focuses the laser to a 0.4-mm spot at a pinhole stop. The second lens images this spot into the plasma. With this arrangement, the laser beam is focused to a 1.3-mm zone in the plasma, a dimension which determines the spatial resolution of the system.

A series of beam stops is arranged along the laser path to reduce stray light. After passing through the plasma and beam stops, the laser is attenuated by two beam dumps. Inside the torch box, a viewing dump is placed across the plasma from the detection optics in an effort to reduce the stray light that enters the detection system.

The following criteria were considered when the scattering geometry was selected. First, the width of the Thomson-scattering spectrum depends on the scattering angle; the larger the angle, the broader the scattering spectrum for a given electron-velocity distribution. In addition, the scattering parameter α is inversely related to $\sin(\theta/2)$ where θ is the scattering angle. It is best to minimize α so the

scattering spectrum is more Gaussian in shape (assuming the electron velocity is Maxwellian). This change in the scattering spectrum is actually related to how "free" the electrons which produce the scattering signal are. For details on this point, see SHEFFIELD [1]. Overall, then, one wishes to maximize the scattering angle. The 135° scattering angle chosen here is a good compromise; at this large angle most of the spectral width and shape advantages are achieved, and instrument crowding is reduced.

2.2 Unique Features of the New Multi-channel System

The major differences between this multi-channel Thomson-scattering instrument and its single-channel predecessor are related to the multi-channel detection system. Other additions include a rotating-mirror optical chopper which provides temporal gating of ICP background radiation in order better to protect the photo-detectors from saturation or damage, and an x-z translation stage which allows selection of the probe volume, and thus spatial mapping of Thomson-scattering measurements. This x-z stage translates the torch housing and impedance-matching assembly both along the laser-beam axis for radial mapping of the ICP and vertically for height profiling of the Thomson-scattering measurements.

The multi-channel detection system, discussed in detail below, segregates the dispersed signal at the exit plane of the spectrometer and simultaneously measures the entire Thomson-scattering spectrum. The chopper assembly, its associated timing electronics, and the three main sections of the multi-channel detection system (i.e., fiber-optic array,

photomultiplier housings and detection electronics) will be described separately.

2.3 Chopper Assembly

A rotating-mirror assembly temporally gates the image of the ICP in order to protect the high-gain photomultipliers from otherwise excessive photocurrents. In earlier work, it was found that even a 2-ms optical gate produced by a mechanical camera shutter permitted ICP background emission to send the PMT into a nonlinear response region [5]. With the present chopper design, the period during which a PMT views the ICP has been reduced by nearly two orders of magnitude to 25 μs. This shortened exposure lessens the likelihood of depleting the charge in the PMT dynode chain, so dynode voltages remain stable and the gains of the tubes are stabilized. The rotating-mirror arrangement was selected over other approaches (e.g. electro-optical devices or fast electronic camera shutters) because of its ability to provide high throughput (90%), large aperture (f/5), and relatively short temporal gate widths (25 μs). Also unlike electronic gating of the PMT supply voltage, the rotating mirror ensures that all channels receive the same gate simultaneously.

Figure 2 shows a simplified diagram of the rotating-mirror assembly. The chopper consists of a 10 x 10-cm flat, front-surface protected-aluminum mirror (Melles Griot, Irvine, CA) which is rotated at 3600 rpm (60 Hz) by a 1/16 hp synchronous AC motor. The mirror rotates in the collimation region between two 25-cm focal-length lenses (Oriel Corp., Stratford, CT). The optical axes of these lenses lie in the plane of rotation of the mirror and are displaced from each other by 45 degrees in that plane. The image of the plasma, which is collimated by

the first lens and focused upon the entrance slit of the monochromator by the second lens, is swept past the entrance slit at a linear displacement velocity of 1.9×10^4 cm/s. Therefore, the 20-mm diameter plasma image passes the entrance slit in about 100 μs. An aperture is positioned in front of the plasma so only about a 5-mm region of the discharge is observed; the optical gate is therefore effectively about 25 μs.

The rotating mirror is housed in a vacuum chamber to reduce air resistance and (even more importantly) to protect the mirror from atmospheric dust and oil vapor. In order to minimize the number of optical surfaces and resulting light losses, the collimating and focusing lenses serve also as windows for this vacuum chamber.

The chopper housing is vertically partitioned into two sections by a light baffle. The scattered radiation transverses the lower section, while the upper part encloses the reflected beam of a He/Ne timing laser (Melles Griot, Irvine, CA). This segregation reduces the chances that stray light from the He/Ne laser will be scattered into the detection optics where it could be observed as stray light. The rotating mirror occupies both vertical sections so the timing and signal beams coincide in time.

In the upper or timing section of the vacuum chamber, two windows are positioned so reflected light from the timing laser falls successively on two optical fibers as the mirror rotates. The first of these fibers carries the He/Ne light to a photodiode which triggers the flash lamp of the ruby laser; light from the second fiber is used to trigger the Q-switch of the ruby laser. Micrometer adjustments locate the position of both fibers to allow accurate and precise timing of these signals with respect to the mirror movement. When these adjustments

are properly made, they guarantee that the laser fires exactly when the mirror is in position to direct the image of the ICP into the entrance slit of the multichannel spectrometer (see following section for details).

An additional design feature of this rotating-mirror assembly is the existence of an enclosed collimated-light region between the detection lenses in which auxiliary optical components such as polarizers, filters, and field stops can be placed. For example, a mica half-wave retardation plate (Melles Griot, Irvine, Ca) is placed in this region to rotate the vertically polarized scattered radiation into the horizontal plane; the efficiency of the monochromator at 700 nm for horizontally polarized light is much greater than for vertically polarized radiation. Additionally, the chopper assembly is anodized black to reduce stray light and multiple reflections of the timing laser.

2.4 Laser Timing

A 2.5-cm mechanical camera shutter (Synchro-Compur, Germany) is positioned in front of the monochromator entrance slit. This mechanical shutter is opened for 1/15 s (about 4 revolutions of the mirror) when the laser is to be fired. Besides providing additional protection for the PMT's, the "X-sync" output of this shutter is used to trigger the electronic timing sequence for firing the ruby laser.

The timing diagram in Fig. 3 clarifies this sequence. Once the camera shutter "X-sync" output has been triggered, the flashlamp is fired on the next pulse from the flashlamp-synchronization photodiode (Fig. 3, trace C) when it receives a signal from its optical fiber. Any previous pulses from the flashlamp-synchronization photodiode are ignored,

and any Q-switch-trigger photodiode pulses which precede the flash-lamp gate are also ignored. After the flashlamp gate, however, the next pulse from the Q-switch synchronization photodiode (Fig. 3, traces D and D') triggers the laser.

Two sequential TTL output pulses are produced by the timing electronics. The first pulse is coincident with the laser pulse, and the second with the Q-switch photodiode pulse (Fig. 3, trace D) on the following mirror rotation (no laser firing accompanies this second TTL pulse). The gated integrators in the multi-channel detection electronics are triggered by these timing pulses for signal (F_1 in Fig. 3) and background (F_2 in Fig. 3) measurements, respectively.

A schematic diagram of the timing circuit which controls the above sequence is shown in Fig. 4. In this diagram, D2 and D3 are the synchronization photodiodes which receive the timing pulses from their respective optical fibers to control the flashlamp and Q-switch triggering, respectively. Transistors T1 and T2 amplify the pulses from photodiodes D2 and D1, respectively. The signals from T1 and T2 correspond to the flash-lamp gate and Q-switch gate (traces C and D) in Fig. 3. The Schmitt-trigger inverters which follow T1 and T2 provide precise triggering pulses. The dual J-K flip-flops Z1 and Z2 (shaded) control the logical sequence of events; the "X-sync" input allows the flashlamp trigger to occur which in turn allows the Q-switch trigger to be produced. Transistor T4 produces a momentary short across output B7, which fires the ruby-laser flashlamp, and transistor T6 produces a 25-50 μs 30-V spike at output B6 to fire the laser Q-switch.

Outputs B2 and B4 provide the TTL logic pulses for external synchronization of the detection electronics to the flashlamp and Q-

switch firing, respectively. For example, the gated integrators are held in reset status by the controlling microprocessor until the flash lamp is fired. The flash-lamp timing pulse at B2 is used to determine when to release this reset status. Output B5 is the "gate" signal and is used to trigger the gate delay modules which produce the integrator gates (the gate delay modules will be described later). Output B3 provides a pulse coincident with the Q-switch photodiode pulse on every mirror rotation. This signal is used as a monitoring point during timing alignment and is unused during normal system operation. Either TTL input B1 or manual switch S1 can be used to reset the timing electronics for another laser firing sequence.

When the calibration switch S2 is in the on position (shorted to ground), monostables Z3 and Z4 produce the synchronized calibration pulse which fires the red light-emitting diode D4 used to normalize the responses of the channels in the detection system. (Transistor T5 produces the current pulse to drive D4.) The first monostable Z3 is used to delay the pulse to the calibration LED D4 so the timing of this light pulse is similar to that of the ruby-laser pulse. This delay is necessary because the external laser-firing circuit produces about a 600-700 ns delay after the Q-switch trigger and before the actual laser pulse. The second monostable Z4 is adjusted to the desired pulse width (400 ns) of the calibration LED.

This calibration sequence occurs repeatedly at the rate of the mirror rotation (60 Hz) while S2 is in the calibration position. In addition, the flashlamp and Q-switch synchronization pulses at B2 and B4 occur continuously as well; as a result, the detection electronics can accumulate a number of LED pulses for improved normalization precision.

2.5 Fiber-Optic Array

The heart of the multi-channel detection system is a 25-channel fiber-optic array. This array, one end of which is mounted at the focal plane of the spectrometer, provides simultaneous multi-channel wavelength measurement. A drawing of the array is shown in Fig. 5. The array was manufactured to specifications by Incon Inc., Southbridge, MA. Each channel is composed of a 2-mm wide by 5-mm high rectangular bundle of 25-μm glass fibers, and leads to a fiber cable (pigtail) of circular cross section and 2 m length. The far ends of the pigtails have connectors which mate with the multi-channel photomultiplier-tube housings. Adjoining channels are separated in the array by 0.5 mm spacers. With the linear dispersion of the J-Y monochromator at 700 nm being 0.18 nm/mm, the spectral bandpass of each bundle is 0.36 nm. The center-to-center channel spacing of 2.5 mm provides an overall channel resolution of about 0.45 nm. The mount which holds the array at the focal plane of the monochromator has adjustments which allow it to be accurately positioned so the focus, wavelength calibration, and tilt of the array can be established easily.

The center channel of the array (channel 13) is nominally positioned at the laser-line wavelength. With this arrangement, the array then provides information on spectral shifts of up to +/- 5.4 nm from this central wavelength. Figure 6 shows how the channels correspond to wavelength location on a hypothetical Thomson-scattering spectrum. The signals from those pairs of channels which are symmetrically located about the center channel (e.g. channels 12 & 14 and 1 & 25) are directed to the same photodetector. Because the Thomson-scattering spectrum should be nearly symmetrical, this approach

doubles the detected signal. To verify this symmetry, shutters located at each PMT housing permit each of the two channels that feed it to be examined separately.

2.6 Multi-channel Photomultiplier Tube Housings

Each output pigtail from the fiber-optic array is connected to one of two seven-channel photomultiplier-tube housings. A drawing of one of these housings is presented in Fig. 7. The PMT in the first position (on the left in Fig. 7a) is used for channel 13. This channel, stationed at the laser wavelength, is used to monitor the Rayleigh-scattering intensity. For this reason, it is provided with attenuators to protect it from the intense Rayleigh scattering. This protection is effected by a slide selector which can position either of two neutral-density filters between the output of the fiber bundle and the PMT. The filters that are ordinarily used have optical densities of 1.0 and 2.0 (Melles Griot, Irvine, CA). This first channel (tube 0) in one of the two multi-PMT housings is not utilized since only one fiber bundle is at the laser wavelength and only 13 channels are required.

The remaining six channels in each of the PMT housings are used for detecting the Doppler-shifted Thomson scattering. As described above, symmetrically located pairs of channels in the fiber array are directed to the same PMT. As shown in Fig. 7a, shutters on tubes 1 through 6 can be used to select the top or bottom group of bundles or both. Channels 14 through 25 are "upper" channels, and channels 1 through 12 are "lower" channels. Accordingly, the selection of upper or lower inputs to the PMTs corresponds to selecting the blue- or red-shifted wings of the Thomson profile, respectively. Although these two wings should be

similar, high electron drift velocity [6,7] and optical features of the spectrometer can make one wing of the spectrum broader or weaker than the other. The present design permits the detection and quantification of this situation.

The lower and upper fiber bundles are attached to each PMT housing at an angle (see Fig. 7b) so the emerging cone of light from the paired bundles illuminates the same region of a respective PMT photocathode. Also, the housings are water-cooled so heat from the dynode bias resistors (about 8 W) does not warm the detectors. In addition, the housings were anodized black to reduce light reflections and leaks, and are rack-mountable for ease of usage and storage.

2.7 Photomultiplier Tube Selection

The photomultiplier tubes employed in this system (Hamamatsu R928) were specified and selected for photocathode radiant sensitivity at 700 nm (better than 40 mAW), photocathode luminous sensitivity (greater than 300 A/lm), and gain (greater than 10^7 at 1000 V bias voltage). Some of the tubes employed far exceed these minimum specifications (see Table 1). The PMTs were arranged, using the value for photocathode radiant sensitivity reported by the manufacturer, with the most sensitive tubes at positions which detect the far wings of the scattering profile. With this arrangment, the weakest signals are detected by the most sensitive tubes.

The dynode-biasing circuit was designed to give the PMTs fast-pulse response, and to provide sufficient charge to reduce saturation problems. A schematic diagram of this circuit is presented in Fig. 8. The increased voltage drop between the photocathode and the first dynode

provides good charge withdrawal from the photocathode and improves the tube's fast-pulse response. The voltage is again tapered upward on the last few stages of the dynode chain to focus the photoelectron charge packet onto the anode and to provide better high-current response.

2.8 Detection Electronics

The detection electronics are comprised of three modules: two banks of eight gated integrators, and a microprocessor-controlled analog-to-digital converter (ADC). Each gated-integrator bank is a rack of eight commercially available gated-integrator cards (Model # 4130A Evans Electronics, Berkeley, CA). A few minor modifications have been made to render these cards more suitable to the present application: 1) the integrating capacitor has been replaced with a 200 pf polystyrene capacitor; 2) the input resistors on both current inputs were replaced by 50-ohm resistors; 3) the voltage-input sections of the cards were disconnected from the summing point of the integrators to eliminate errors produced by offsets and noise in these unused input stages; 4) connections were added to the inverting inputs of the final output operational amplifiers. This last change allows the gains of the output amplifiers to be increased if desired.

The analog-to-digital converter/integrator-control module is based on a board-level 6502 microprocessor that runs at a clock frequency of 2 MHz (Model 7510 Cubit Division, Proteus Industries, Mountain View, CA). The microprocessor has control over all functions on the gated integrators and their companion gate-delay modules (located in the control module).

The gate width of the integrators can be adjusted under computer control from 100 ns to almost 1 ms in 100-ns increments. Each of the eight channels in each of the integrator modules can be switched under computer control to use any one of four different gate sources. These four sources include signals produced by either of two gate-delay cards (Model #4145-2, Evans Electronics, Berkeley, CA), referred to below as "gate A" and "gate B", a trigger from an external source, or a "software" gate generated by timers on the microprocessor.

Output voltages from the gated-integrator cards are digitized by a 16-channel 40-kHz ADC module (model # DT5712 Data Translation Inc., Marlboro, MA). The microprocessor has complete control over this ADC and can read and store conversion data in a 48 k random-access memory buffer. The data can then be transferred over a serial line at 19.2 kbaud to a host computer. The computer used in this study to accept data and send control information to the 6502 microprocessor is an IBM 9000 laboratory computer (IBM Instruments Inc., Danbury, CT).

2.9 Other Hardware

The radio-frequency power supply used to sustain the ICP is a 2.5 kW, 27.12 MHz generator (Plasma Therm model HFP 2500). All gas flows were metered by a mass-flow controller (Tylan, Carson, CA). The ICP torch was a demountable version of the low-flow, low-power design described by REZAAIYAAN and HIEFTJE [8]. The ruby-laser head was cooled with 15°C deionized water from a recirculating cooler (Neslab Model # RTE-5B, Neslab Instruments Inc., Newington, NJ).

The stray-light rejection capability of the instrument was evaluated with the aid of a gas restrictor mounted on top of the ICP

torch (Fig. 9). This restrictor is used to provide a pocket of atmospheric-pressure gas, and is useful even with lighter gases such as helium. The device can be positioned to allow scattering signals to be measured at vertical heights from 7.5 mm above the load coil (ALC) to 25 mm ALC. It is made of black anodized aluminum to reduce its effect on the measured stray-light signals and has a 10-mm gap around the laser path which provides clearance for the 1.3-mm laser beam. The restrictor is small enough to contain a flowing gas stream and minimize infusion of atmospheric gases.

Scattering measurements with this gas restrictor were made over a range of helium flow rates to determine the flow necessary to produce an atmospheric-pressure helium pocket inside the restrictor (Fig. 10). The resulting curve is what one would expect. As the helium flow is increased, the scattering signal rapidly decreases; the Rayleigh cross-section of helium is more than 50 times smaller than that of air, and the helium displaces the air in the scattering volume. At a flow rate of 10-12 l/min helium, the scattering signal reaches a minimum, and then slowly increases at higher flow rates. This increase is probably caused by scattering from turbulence that occurs at the higher flow rates.

The two sets of flow conditions chosen for evaluating stray light in the instrumental system are 10 l/min argon introduced into the outer-flow port of the ICP torch and, secondly, a total of 12 l/min helium, 10 l/min of which is introduced into the outer-flow port, and 2 l/min into the intermediate-flow port of the ICP torch. No central flow was used in either case. Note that the argon flow rate is not critical since the Rayleigh-scattering cross section of air is almost identical to that of

argon, so incomplete displacement of the air would produce very little error in the scattering signal.

3. SYSTEM EVALUATION

3.1 Stray-Light Rejection

The most important consideration in evaluating the instrument concerns its ability to reject stray light. All sources of stray light increase the background received by the detection optics and monochromator; this background complicates calibration and increases noise. Moreover, any monochromator has a finite contrast and will spread some of the light at the laser wavelength across other, presumably Doppler-shifted, channels.

Even in the most carefully designed instrument, Rayleigh scattering from the plasma gases will pose a theoretical minimum to the detected stray light in a Thomson-scattering measurement. A comparison of the instrumental performance to this theoretical limit is, therefore, informative. If one estimates the gas temperature in the plasma and thus the argon number density at atmospheric pressure, one can determine approximately the portions of the detected signal which are due to Rayleigh scattering and to other sources of stray light [4].

One approach to making this estimate was used to evaluate the single-channel instrument designed earlier in our laboratory [4]. In this approach, the signal obtained at the laser wavelength with the plasma ignited is compared to the signal observed with the plasma off. Because the Thomson-scattering component at the laser wavelength can be neglected, both signals are essentially comprised of Rayleigh scattering

and stray light; a difference between the two signals arises only from reduced Rayleigh scattering at the lower gas density in the hotter plasma. Because the gas density difference can be estimated by assuming a certain plasma-gas temperature, the relative contributions from stray light and Rayleigh scattering can be calculated.

If S_{on}, S_{off}, and S_s are the Rayleigh-scattering signals with the ICP on and off, and the stray-light signal, respectively, the ratio R

of the signal when the ICP is off to that observed from a lighted plasma is

$$R = \frac{S_{off} + S_s}{S_{on} + S_s} = \frac{n_{off} + n_s}{n_{on} + n_s} \qquad (1)$$

where n_{off} and n_{on} are the argon atom number densities at room temperature and at the plasma temperature, respectively. The equivalent argon number density that would yield a Rayleigh-scattering signal equal to the stray-light level is denoted n_s. At atmospheric pressure, the argon number density is, of course, inversely proportional to the gas temperature so that

$$n_{on} = n_{off} \frac{T_{off}}{T_{on}} \qquad (2)$$

where T_{off} is room temperature (300 K) and T_{on} is the gas temperature in the plasma.

In the present multi-channel system, scattering signals have been found to be more than 20 times lower from the ignited plasma than from room-temperature argon. This ratio would require that the plasma temperature be in excess of 6000 K for there to be any stray light

contribution at all. This high a gas temperature might indeed exist in the ICP [9-11]. Nonetheless, it is clear that stray light in the new multi-channel system is about as low as in the earlier single-channel version [4].

Of course, it would be desirable to use a method of determining stray light which is independent of an assumed gas temperature in the ICP. One such alternative method involves using two or more gases with different Rayleigh scattering cross-sections. Again, the difference in the measured scattering signals for the various gases will be due to the changes in the Rayleigh component. The magnitude of the stray-light component can then be obtained from the negative x-intercept of a plot of scattering intensity vs. equivalent argon pressure (or number density). The units of the stray-light component will be the same as the ones used on the gas pressure axis. For example, if measured total (Rayleigh + stray-light) intensity is plotted against equivalent argon gas pressure in torr, the units of the calculated stray-light level will be in torr argon. In other words, the stray light is then equivalent to a Rayleigh-scattering signal from a specified pressure of argon.

In the present investigation, helium was chosen as the second gas. A He flow rate into the gas restrictor of 12 l/min was used to maintain an atmosphere of helium in the scattering volume. For the instrument described here, the ratio of the scattering signal from argon to that obtained with helium as the scattering gas is usually between 30-40. This ratio corresponds to an equivalent stray-light level of from 13-7 torr argon, respectively. This is an acceptably low stray-light level, and means that the instrument should be able to make Thomson-scattering measurements without significant problems with stray light. In

addition, this value is similar to the 14-torr argon stray-light level measured for the single-channel system with an assumed 6000 K plasma gas temperature. Variations in the measured stray-light component in the new multi-channel system seem to be related to system alignment; when the scattering system is in good alignment, the stray-light level is low.

In an atmospheric-pressure plasma with a 6000 K gas temperature, the Rayleigh-scattering signal is equivalent to that from a room-temperature argon gas pressure of 38 torr. Therefore, the stray light from sources other than Rayleigh scattering is about 25-30% of the Rayleigh contribution. Experience with the multi-channel system indicates that the first Doppler-shifted channel receives a stray-light component of about 1/1000th the intensity of the channel at the laser wavelength (the Rayleigh channel). In addition, the magnitude of the Thomson-scattering signal in the first shifted channel is expected to be about 1-5% of the intensity of the Rayleigh channel. Therefore, the total stray-light contribution to the Thomson-scattering signal of this first channel is between 2-10% of the signal.

All other Doppler-shifted channels receive far less stray light than the first shifted channel. The stray-light level found in the multi-channel system is therefore low, and the system is capable of providing Thomson-scattering measurements without significant errors caused by stray light. Moreover, the residual stray-light contribution can be and has been subtracted from the Thomson-scattering data. The stray-light spectrum obtained from Rayleigh scattering in <u>room-temperature</u> argon has been plotted in Fig. 11 on the same scale used to display the Thomson-scattering data presented later in Fig. 13. Comparing these plots, one can

conclude that the stray-light contribution to the Thomson data is small. Also, one notes from Fig. 11 that the instrumental bandwidth should not contribute appreciably to a measured Thomson-scattering spectrum.

3.2 System Calibration

Probably the most difficult problem that is faced in using the multi-channel system is compensation for channel-to-channel variations. Unless the relative channel responses are normalized, the resulting Thomson-scattering spectra are almost meaningless (see Fig. 12).

The preferred approach to normalizing the channels would be to monitor simultaneously a spectrally flat emission source that has the same temporal profile as the ruby laser. The relative responses of all channels could then easily be deduced. Unfortunately, a pulsed source (25 ns) with a flat response over the wavelength range of interest (690-700 nm) is not readily available, and a DC source does not provide accurate relative-response data since the temporal response of the individual PMTs probably differs substantially.

A red, pulsed light-emitting diode (LED) (Toshiba Electronics Manf.) has been used here for channel normalization. This diode has a broad (> 100 nm) emission band centered at 700 nm and with the driving circuit used it produces a minimum pulse width of about 400 ns, about 16 times longer than the ruby laser pulse. The LED is positioned above the second concave (focusing) mirror in the Czerny-Turner spectrometer and illuminates the fiber-optic array directly; consequently, the breadth of its emission band is important only insofar as it affects the different wavelength response of individual photodetectors. Normalization performed with this LED appears to be reliable. Table 2 lists typical normalization

factors, and Fig. 13 shows the effect of the normalization on the data of Fig. 12.

3.3 Thomson-scattering Spectra

Figure 13 is a normalized Thomson-scattering spectrum obtained with the new multi-channel scattering instrument. It was obtained from an 875 watt ICP at 5 mm above the load coil (ALC) and 3 mm off axis. Because the spectrum is symmetrical, only one half of it need be displayed. The intensities on the ordinate are actually scattering ratios (i.e. the scattering signal is ratioed to the laser power). The spectrum is displayed as a histogram because the fiber-optic array separates the scattering signal into individual wavelength segments. Also, because the array has a spacer between each pair of its channels, there are gaps in the scattering spectrum.

As mentioned earlier, under the proper plasma and instrumental conditions, the Thomson-scattering spectrum should be Gaussian in shape. The curve drawn over the data histogram in Fig. 13 is the calculated Thomson-scattering spectrum corresponding to a plasma with a 9100 K (0.79 eV) electron temperature and an electron number density of 1.1×10^{15} cm^{-3}. Although the fit is not perfect, it appears that the experimental spectrum has a Gaussian shape.

The relative standard deviation (RSD) of the data displayed in Fig. 13 ranges from about 10% in the high-intensity center channels to more than 100% in the weaker wings of the scattering spectrum. These deviations were obtained from 10 separate measurements. Unfortunately, the large variation in signals obtained in the weaker protions of the scattering spectrum complicate data analysis. Electron concentrations

calculated from such a spectrum are fairly reliable since they are computed from the area under the curve, and the wings of the spectrum (where the largest variations occur) do not greatly affect the values. In contrast, electron temperatures are determined by the width and shape of the Gaussian curve, and are strongly affected by the points in the wings. Temperatures calculated from these data are therefore not yet as reliable as desired.

The limiting noise in the present system seems to be statistical or quantum noise. From the voltages measured by the ADC, the charge retained on the 200-pf integrating capacitors has been calculated. From this value, and an assumed PMT gain of 10^7, it is estimated that 60 photons produced the signals represented by the larger histogram bars in Fig. 13. The theoretical RSD for such a signal is 13%, similar to the standard deviations observed.

For the signals in the wings of the spectrum, instrumental variations are probably important also. The estimated number of photons that produces these smaller signals is very low (about 4 photons), and the theoretical RSD should be about 50%. The measured RSD in excess of 100% might be produced by variations in the plasma, in the measuring instrument, or by the inherent uncertainty in a standard deviation. At these low-signal levels, switching and leakage currents in the integrator circuits could easily account for the observed variation. It is important that any significant increase in the number of photon events would greatly reduce these uncertainties. Such an increase would probably result from the use of a higher-power, more conventional ICP which is known to possess a higher electron number density [5] than the

plasma employed here [8]. Future work will involve the examination of such a source.

4. Conclusion

The new multichannel Thomson-scattering is capable of providing adequate resolution, low stray light, and nearly photon-limited spectra. As a result, the instrument provides reliable values for electron concentrations, which are proportional to the integrated spectrum and therefore depend most strongly on strong and therefore precise intensities that are in the center of the spectrum. In contrast, computer electron temperatures rely most heavily on less intense and less precise intensity values on the wings of the scattering spectrum. Therefore, electron temperatures reported here must be considered to be only approximate.

Another factor which limits reliability of the reported values is the difficulty encountered in normalization of individual channels in the new instrument. We are not yet confident that the light-emitting diode employed here provides a sufficiently precise or reliable calibration. Unequal illumination of various channels by light scattered within the spectrometer might produce a normalization factor that differs from that which would be appropriate for light that entered the spectrometer in a conventional manner.

In the future, these problems will be alleviated by the use of an alternative laser source and adoption of a new normalization procedure. Because measured values on the wings of the Thomson-scattering spectrum are currently limited by photon statistics, we will incorporate a rapidly pulsed (20 Hz) Nd:YAG laser into the system. Because the average light flux from this new source is far greater than is available from the current ruby

laser, signal magnitudes and precision should improve accordingly. In addition, we will substitute for the LED-based normalization approach and externally driven continuum lamp which will be "gated" by the rotating mirror already present in the instrument. It is anticipated that this normalization method will approach more closely conditions that are experienced by real Thomson-scattered radiation. Finally, we intend to improve signal-to-noise ratios through use of a photodetector-gating scheme. Such an approach will enable each photomultiplier to experience background radiation from the ICP for a much shorter period of time and should improve photodetector linearity, reduced fatigue, and minimized detected background.

ACKNOWLEDGEMENT

The authors would like to thank George Ewing for his generous loan of the ruby laser used in this investigation. Supported in part by the National Science Foundation through grant CHE 83-20053, by the Office of Naval Research, and by American Cyanamid.

REFERENCES

[1] J. Sheffield, Plasma Scattering of Electromagnetic Radiation, Academic Press, New York (1975).

[2] W. Lochte-Holtgreven, Plasma Diagnostics, Ed. W. Lochte-holtgreven, p. 135, North-Holland, Amsterdam (1968).

[3] K. A. Marshall and G. M. Hieftje, Spectrochim. Acta 43B, 000 (1988).

[4] M. Huang, K. A. Marshall and G. M. Hieftje, Spectrochim. Acta 40B, 1211 (1985).

[5] M. Huang, K. A. Marshall and G. M. Hieftje, Anal. Chem. 58, 207 (1986).

[6] D. S. Douglas and R. S. Houk, Prog. Anal. Atom. Spectrosc. 8, 1 (1985).

[7] J. J. A. M. van der Mullen, Excitation Equilibria in Plasmas, Ph.D. Thesis, Eindhoven University of Technology, Eindhoven (1986).

[8] R. Rezaaiyaan and G. M. Hieftje, Anal. Chim. Acta 173, 63-75 (1985).

[9] H. G. C. Human and R. H. Scott, Spectrochim. Acta 31B, 459-73 (1976).

[10] T. Hasegawa and H. Haraguchi, Spectrochim. Acta 40B, 123-33 (1985).

[11] K. A. Marshall and G. M. Hieftje J. Anal. Atom. Spectrom. (in press, 1987).

Table 1

R928 Photomultiplier Tube Sensitivities

Position	Array Channels	Serial Number	Cathode Luminous Sensitivity (μA/lm)	Cathode Radiant Sensitivity (mA/W)	Gain ($\times 10^7$)
A0	--	--	--	--	--
A1	12,14	YL 5841	337	40	1.0
A2	11,15	YL 791	340	40	1.7
A3	10,16	YL 2751	360	40.5	1.4
A4	9,17	YT 8572	340	41.1	1.2
A5	8,18	YL 3157	360	41.5	2.3
A6	7,19	YL 541	350	43.5	1.0
B0	--	--	--	--	--
B1	6,20	YT 5844	390	43.7	2.1
B2	5,21	YL 5810	412	44	1.5
B3	4,22	YU 349	369	48.5	2.7
B4	3,23	YU 483	368	81	1.2
B5	2,24	YU 670	352	81	1.3
B6	1,25	YL 5406	383	83	1.2

Note the cathode radiant sensitivity was measured at 700 nm. Positions A0 and B0 do not have R928's from this lot and these specifications were therefore not supplied by Hamamatsu. All specifications above were measured by Hamamatsu.

Table 2

Typical Multi-Channel Normalization Factors

A/D Channel Number	Array Channel Numbers	Normalization Factors
0	13	31
1	12,14	5.4
2	11,15	3.7
3	10,16	3.1
4	9,17	9.3
5	8,18	1.7
6	7,19	6.1
9	6,20	1.0
10	5,21	2.9
11	4,22	1.4
12	3,23	4.2
13	2,24	4.8
14	1,25*	3.9

* The 14th A/D integrator channel is presently used to monitor the laser power photodiode.

FIGURE CAPTIONS

Figure 1. Block diagram of the entire multi-channel Thomson-scattering apparatus. Alphabetically labeled components are:

A) the laser focusing lenses and pinhole aperture,

B) the first beam-stop box,

C) the torch housing and impedance-matching box on the x-z translation stage,

D) the second beam-stop box,

E) the first beam dump (in which the photodiode to monitor the laser power is mounted),

F) the second Brewster's angle beam dump,

G) the camera shutter, and

H) the fiber-optic array and output pigtails.

Figure 2. Cut-away drawing of the rotating-mirror assembly. The baffling of the mirror container between the upper (timing) section and lower (signal) section is apparent.

Figure 3. Timing diagram of the laser-firing and signal-integration sequence. Note that both a signal (F_1) and ICP background (F_2) integration are performed.

Figure 4. Timing circuit which controls the laer-firing and signal-integration sequence. See text for details.

Figure 5. 25-channel fiber-optic array. Each channel is 5-mm high by 2-mm wide; a 0.5-mm spacer is located between each pair of channels. Each channel accepts approximately a 0.36 nm window of the Thomson-scattering spectrum. Adjacent channels are separated by about 0.45 nm.

Figure 6. Depiction of how a hypothetical Thomson-scattering spectrum falls on the fiber-optic array. A wavelength axis is supplied to clarify the wavelength coverage of the array.

Figure 7. Drawing of one of the two seven-channel photomultiplier-tube housings. Part a of this figure is a front view and part b is a side view.

Figure 8. The dynode-biasing circuit used for each PMT where R1 = 49.9 kΩ, R2 and R10 = 200 kΩ, R3-R9 = 100 kΩ, R11 = 300 kΩ, C1-C3 = 0.1 μf, K is the photocathode, A is the anode, and DyN is dynode number N.

Figure 9. Gas restrictor which when mounted on top of the ICP torch is used to provide a pocket of gas for Rayleigh-scattering measurements of room-temperature gases. It is needed particularly for lighter gases such as helium.

Figure 10. Effect of the flow rate of helium into the gas restrictor on measured Rayleigh-scattering intensity. At helium

flow rates above 5 l/min atmospheric gases appear to be displaced entirely from the probe volume.

Figure 11. A plot of the Rayleigh-scattering (background) intensities from room-temperature argon. Note that the signals have been scaled to correspond to that used in Figure 13; a comparison of these two figures shows the relative contribution of Rayleigh scattering to the Thomson-scattering spectum.

Figure 12. Raw (non-normalized) Thomson-scattering data. Here and in the spectrum of Fig. 13, the channel shifted approximately 3 nm from the incident laser line appears to be zero because it lies at a strong argon emission wavelength. As a consequence, the channel is saturated during both signal (Thomson) and background measurements and is reduced to zero during background subtraction.

Figure 13. Spectrum of the same data shown in Figure 12 after normalization. These data were obtained from an 875-watt plasma at 5 mm ALC and 3 mm off axis. The curve drawn over this histogram is a calculated scattering spectrum for a 0.79 eV electron temperature and a 1.1×10^{15} cm^{-3} electron concentration.

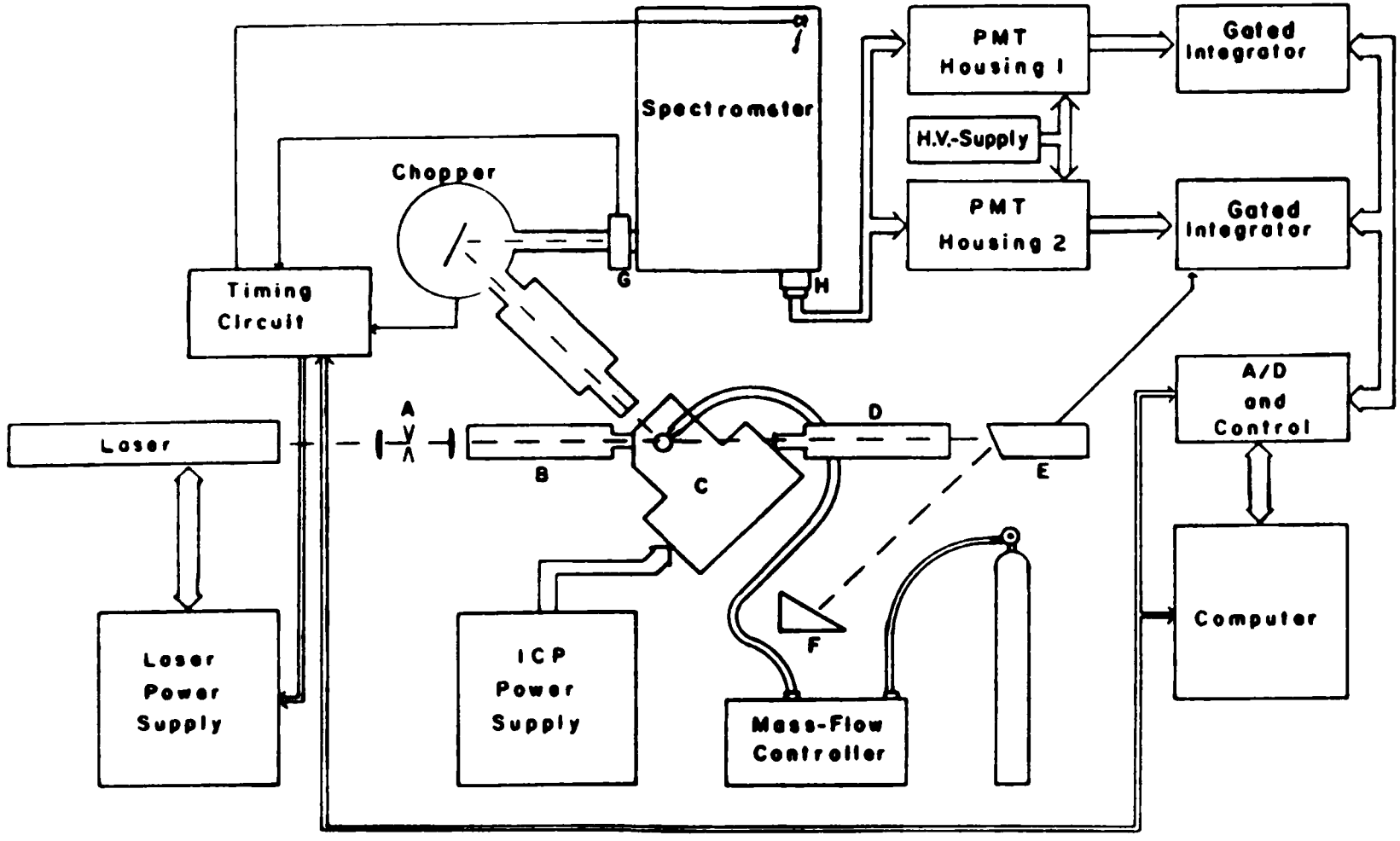
Spectrometer
PMT Housing 1
Gated Integrator
H.V.-Supply
PMT Housing 2
Gated Integrator
Chopper
Timing Circuit
G
H
A/D and Control
A
D
Laser
B
C
E
Computer
Laser Power Supply
ICP Power Supply
F
Mass-Flow Controller

Fig. 1

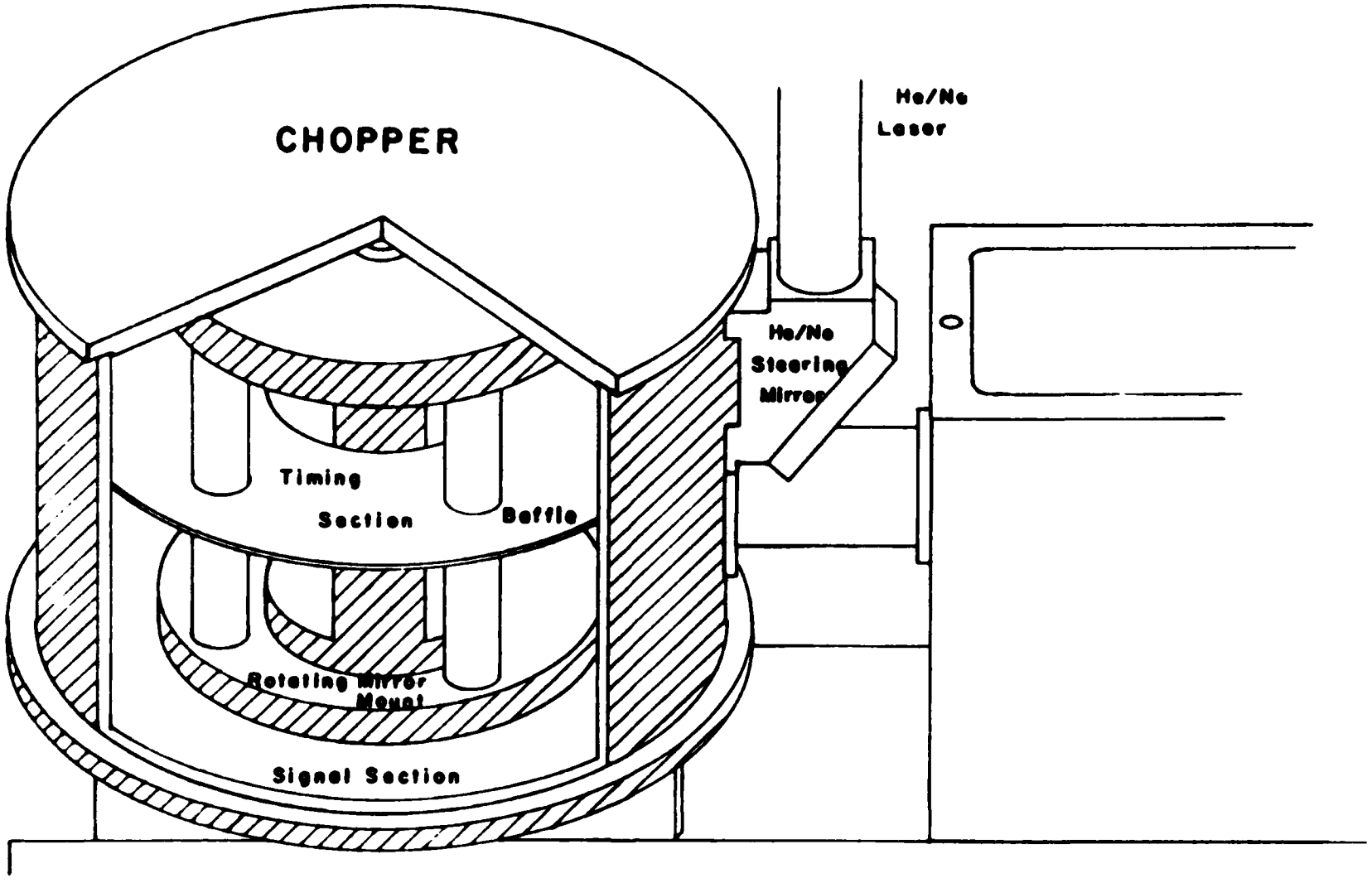
CHOPPER
He/Ne
Laser
He/Ne
Steering
Mirror
Timing
Section
Baffle
Rotating Mirror
Mount
Signal Section

Fig. 2

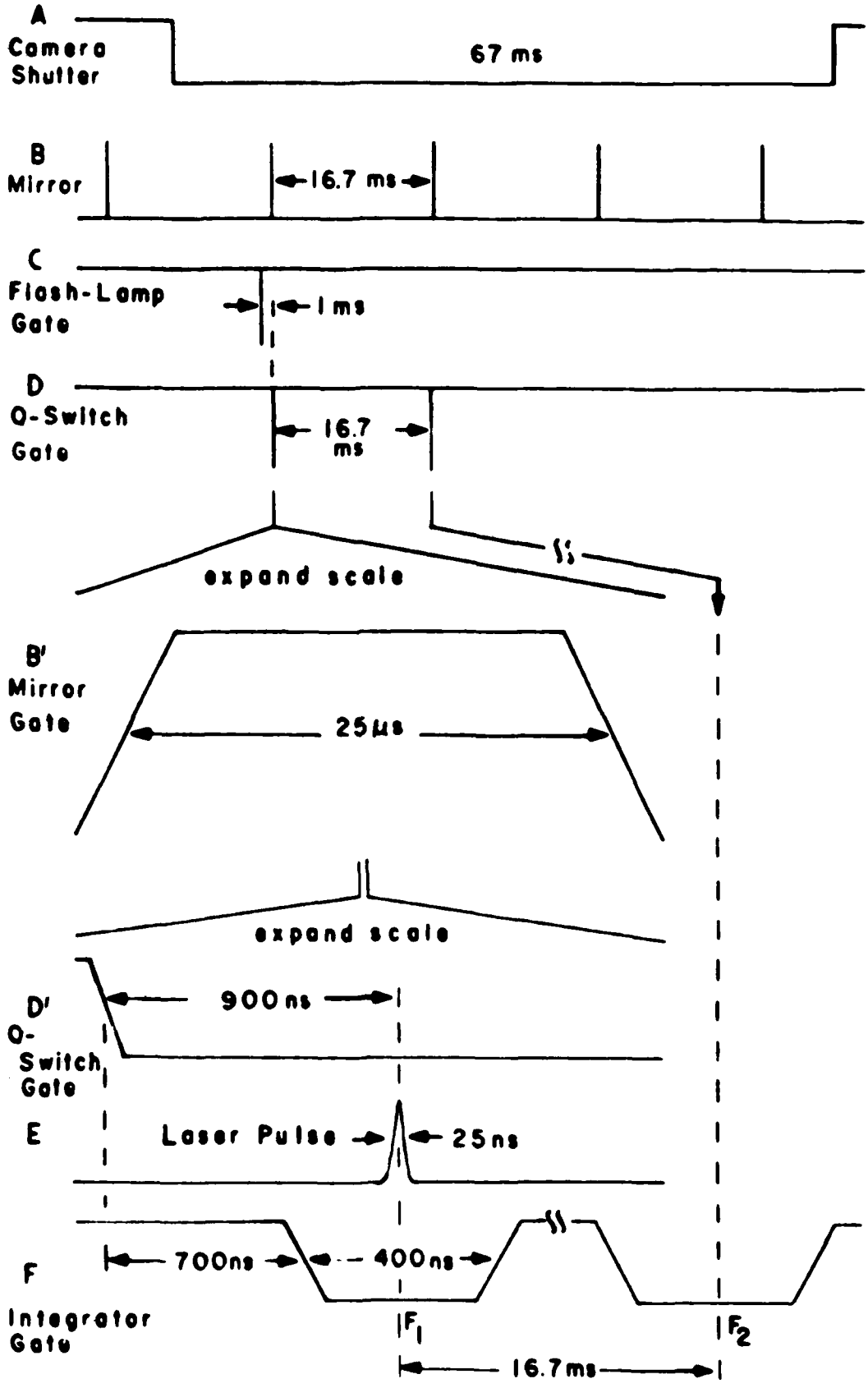
A
Camera
Shutter
67 ms
B
Mirror
16.7 ms
C
Flash-Lamp
Gate
1 ms
D
Q-Switch
Gate
16.7
ms
expand scale
B'
Mirror
Gate
25μs
expand scale
D'
Q-
Switch
Gate
900 ns
E
Laser Pulse
25 ns
F
Integrator
Gate
700ns
400ns
F1
F2
16.7ms

Fig. 3

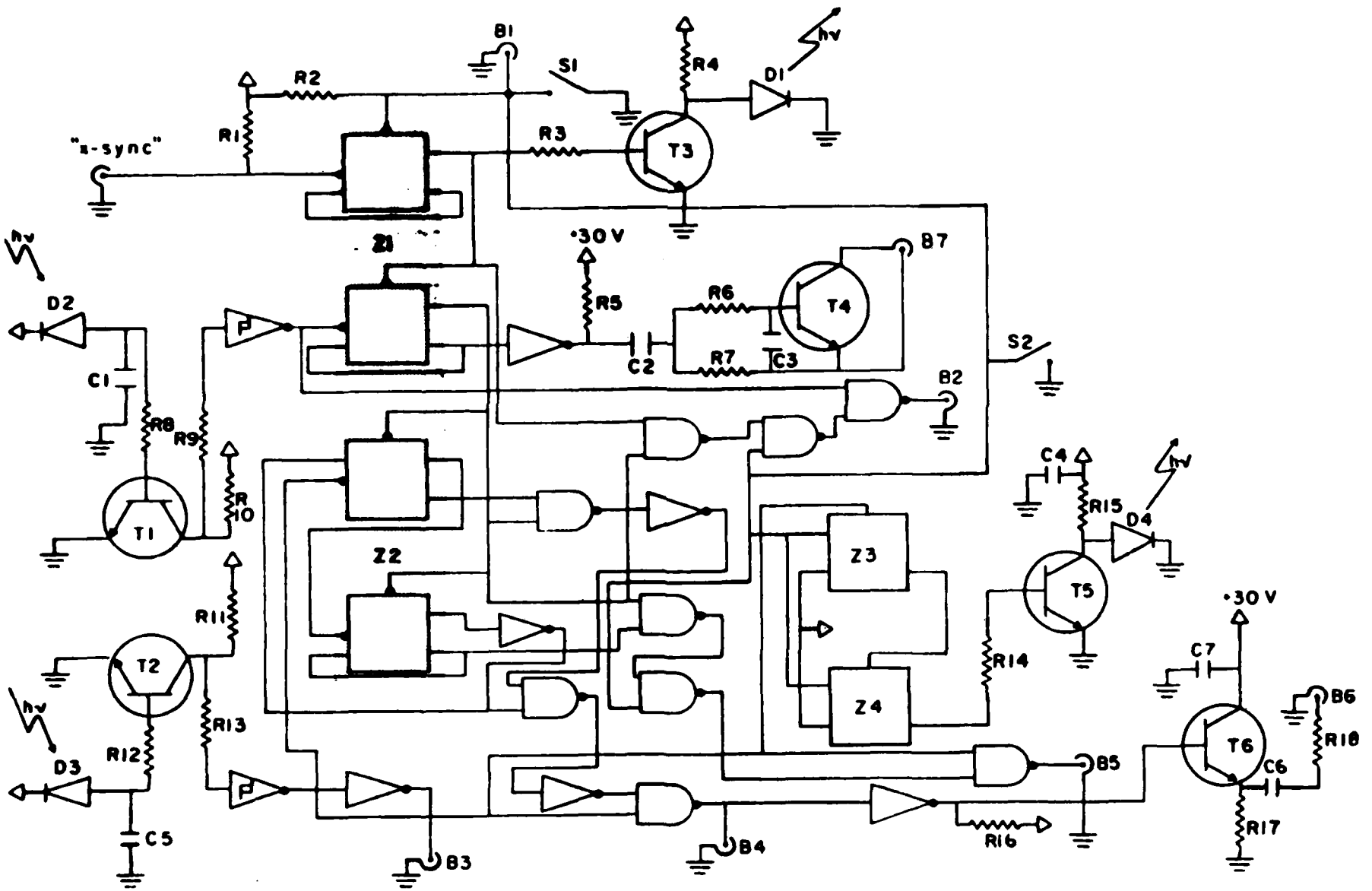
B1
S1
R4
D1
hv
R2
R1
"x-sync"
R3
T3
Z1
+30 V
B7
R5
R6
T4
S2
D2
C2
R7
C3
B2
C1
R8
R9
P
R10
T1
Z2
Z3
C4
R15
D4
T5
+30 V
R11
Z4
R14
C7
T2
B6
R18
R13
T6
R12
D3
B5
C6
C5
R16
R17
B3
B4

Fig 4

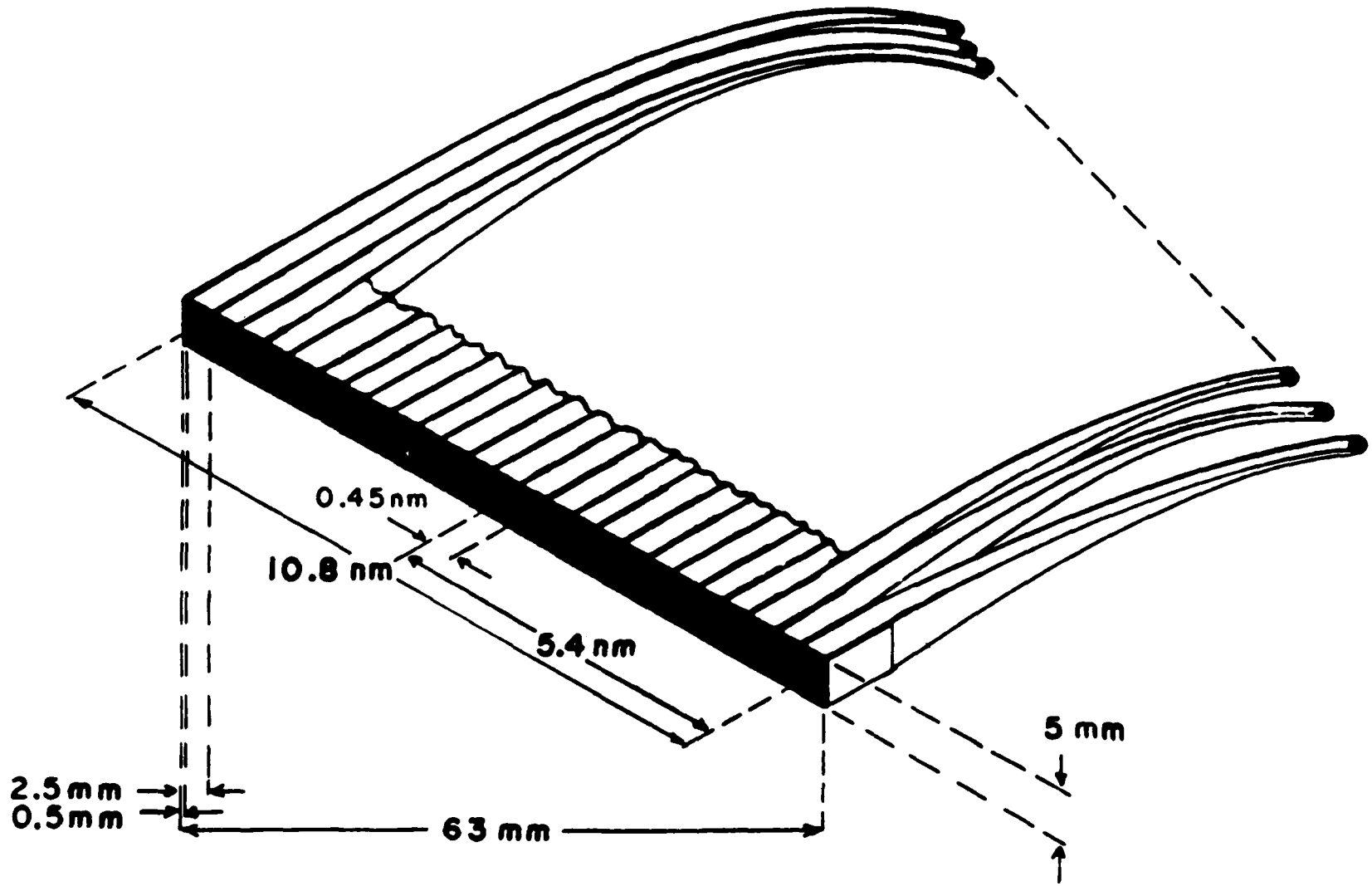

Fig. 5

Fig 6

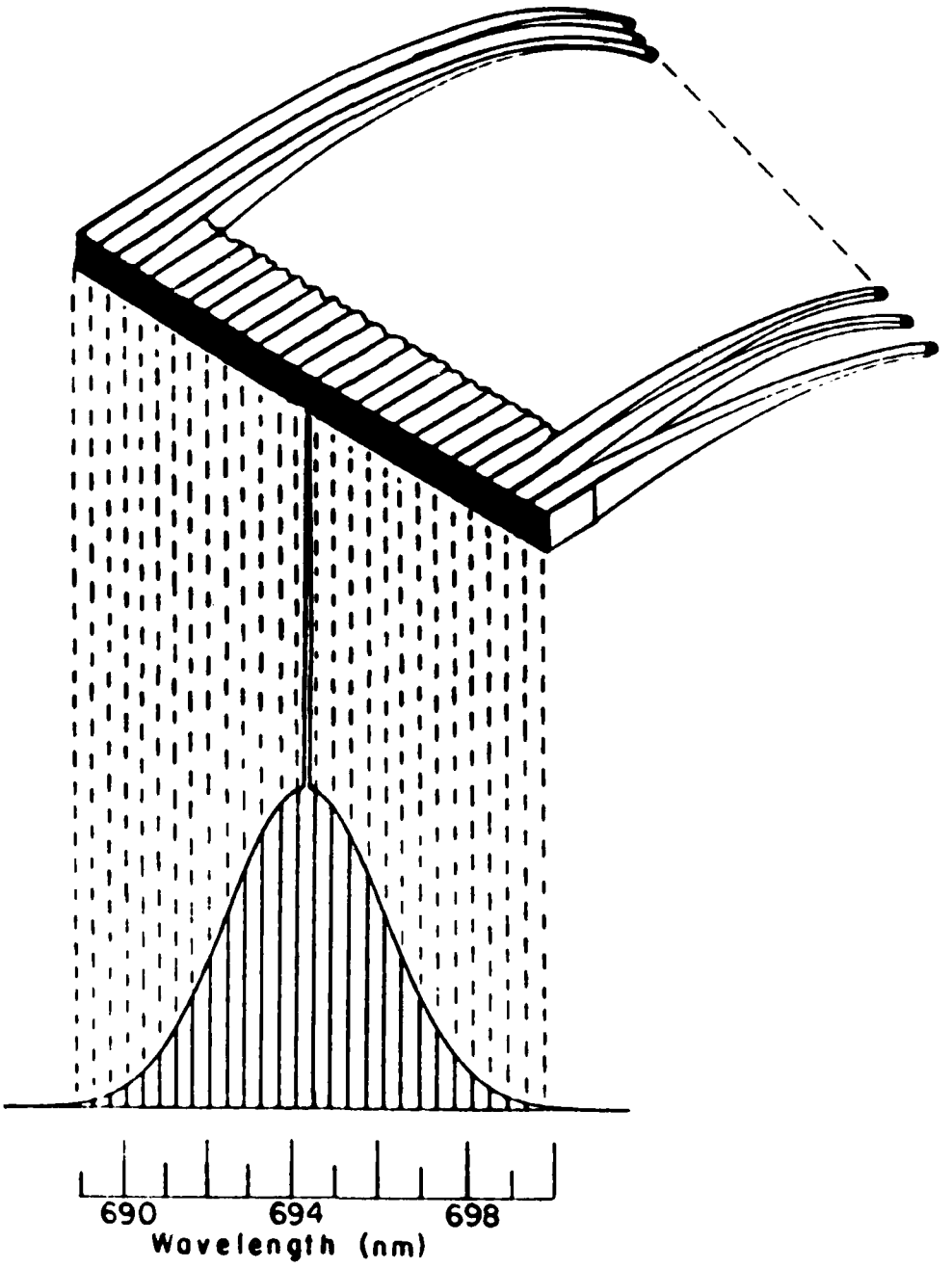

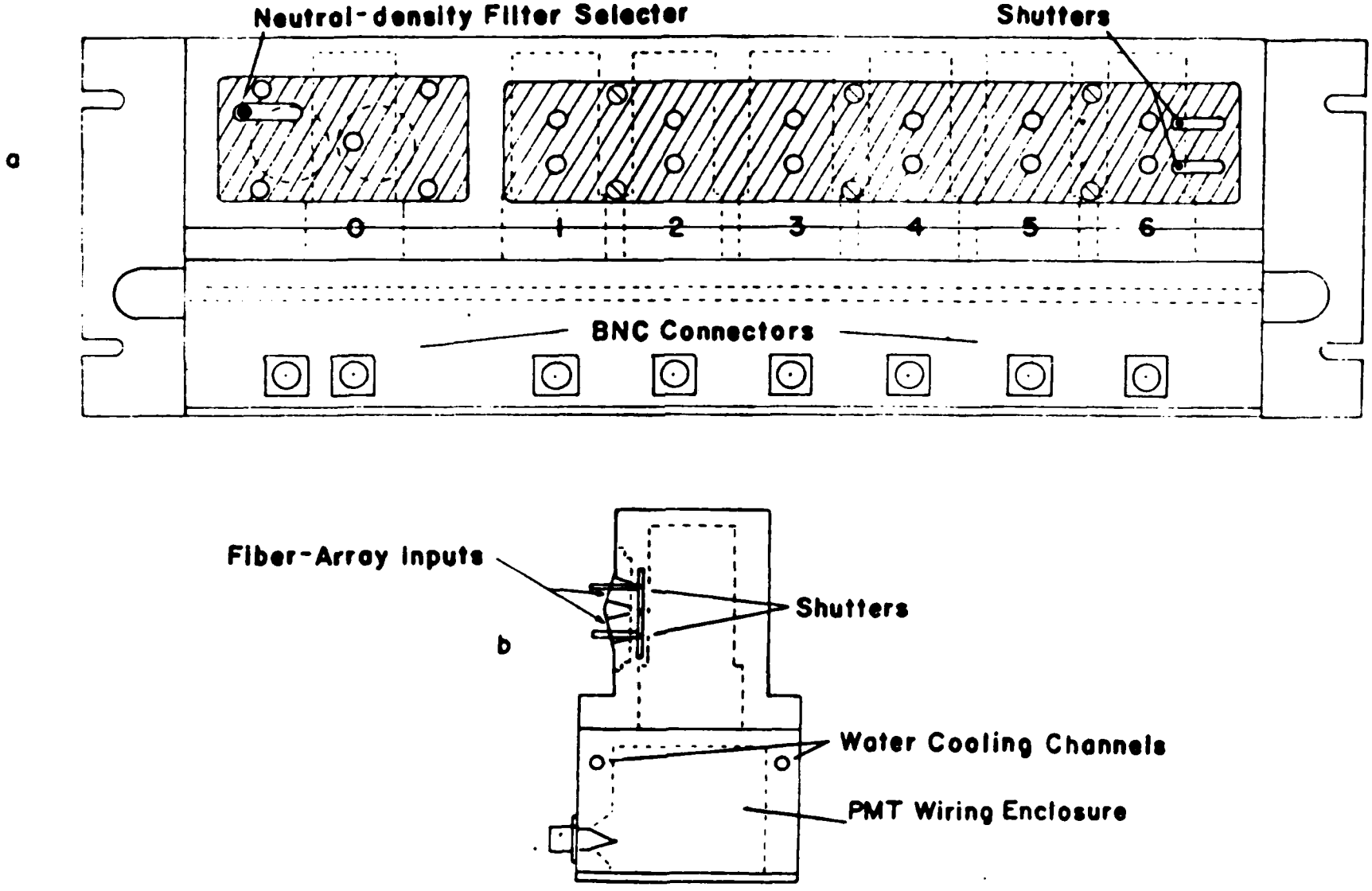
a
Neutral-density Filter Selector
Shutters
0
1
2
3
4
5
6
BNC Connectors
b
Fiber-Array Inputs
Shutters
Water Cooling Channels
PMT Wiring Enclosure

Fig 7

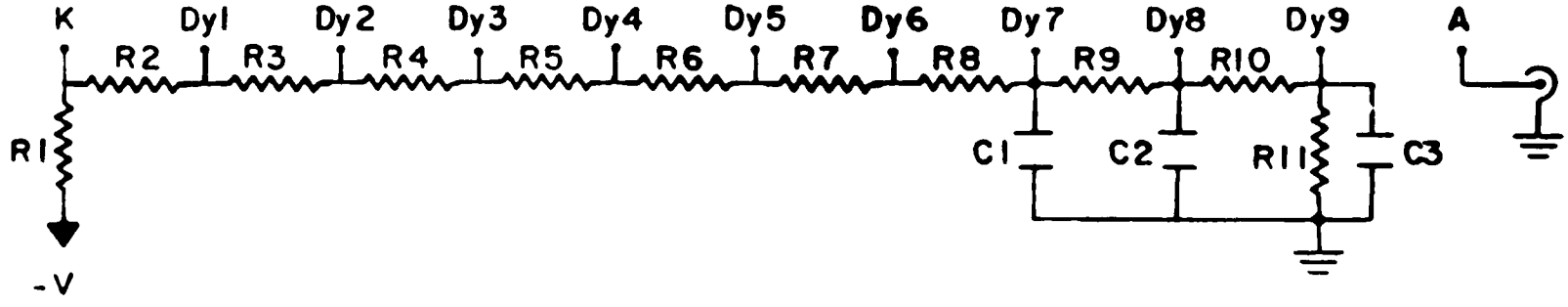
K
Dy1
Dy2
Dy3
Dy4
Dy5
Dy6
Dy7
Dy8
Dy9
A
R2
R3
R4
R5
R6
R7
R8
R9
R10
R1
C1
C2
R11
C3
-V

Fig. 8

Fig. 9

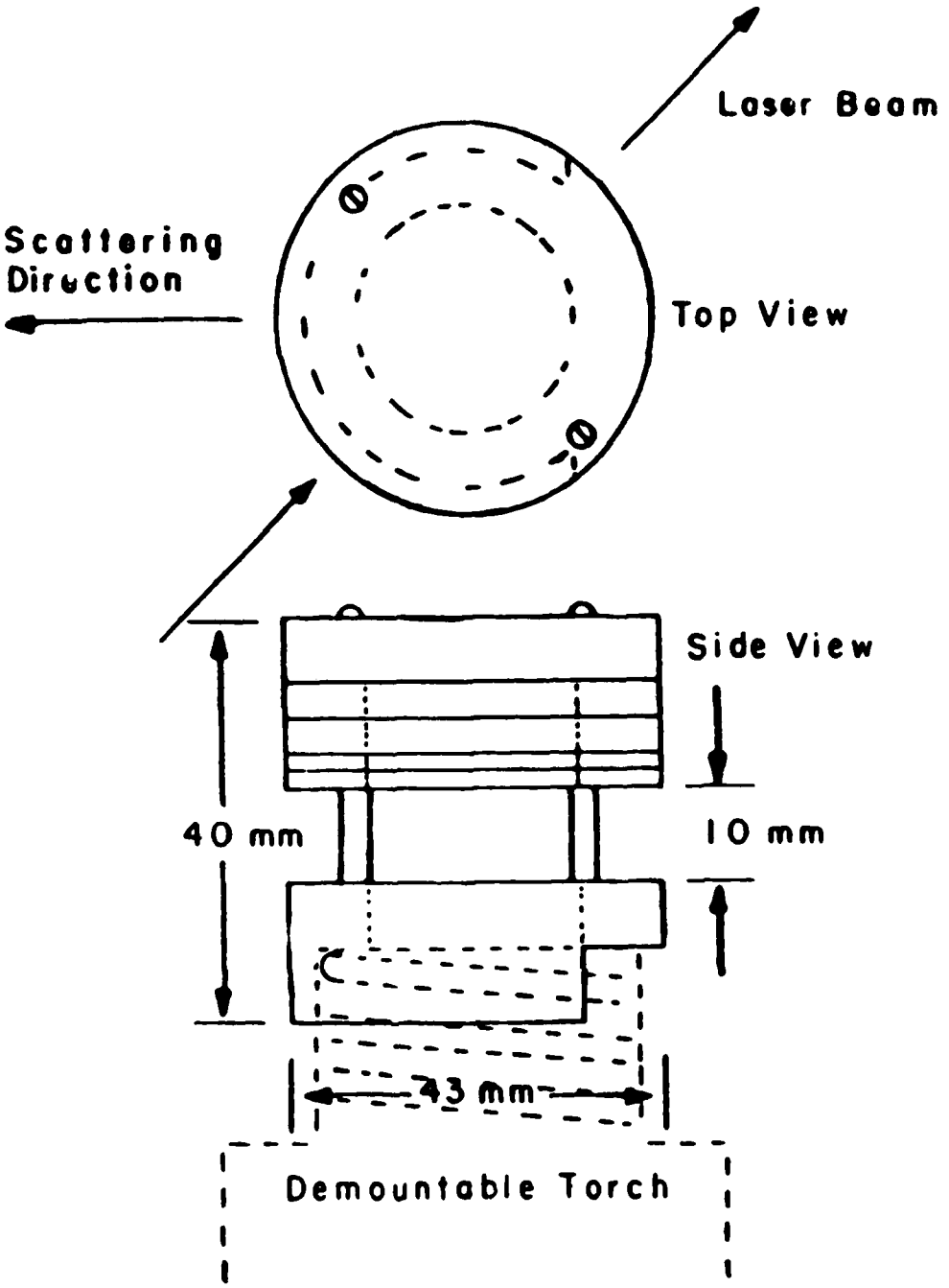
Laser Beam
Scattering Direction
Top View
Side View
40 mm
10 mm
43 mm
Demountable Torch

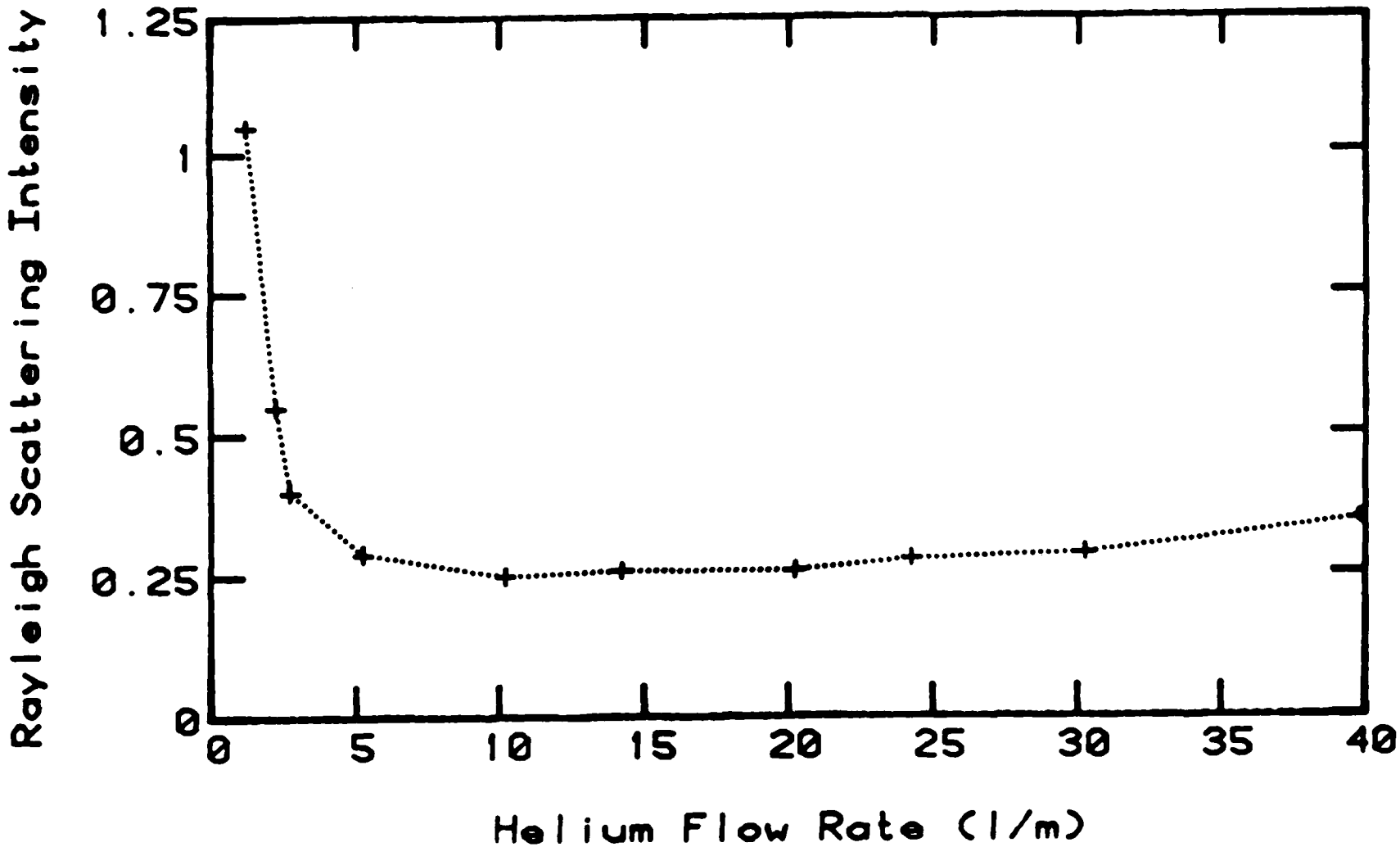
Rayleigh Scattering Intensity
1.25
1
0.75
0.5
0.25
0
0
5
10
15
20
25
30
35
40
Helium Flow Rate (l/m)

Fig. 10

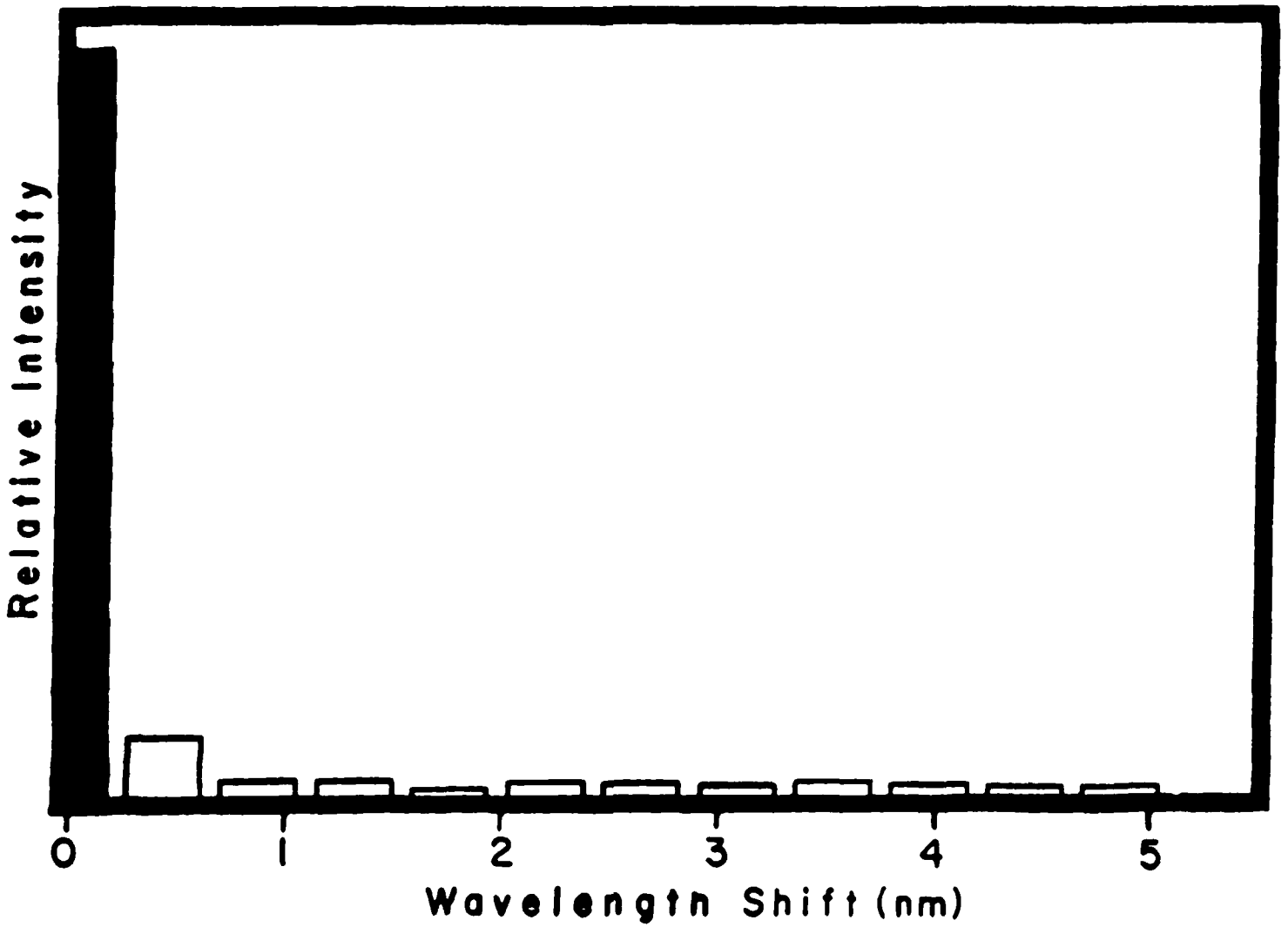

Fig. 11

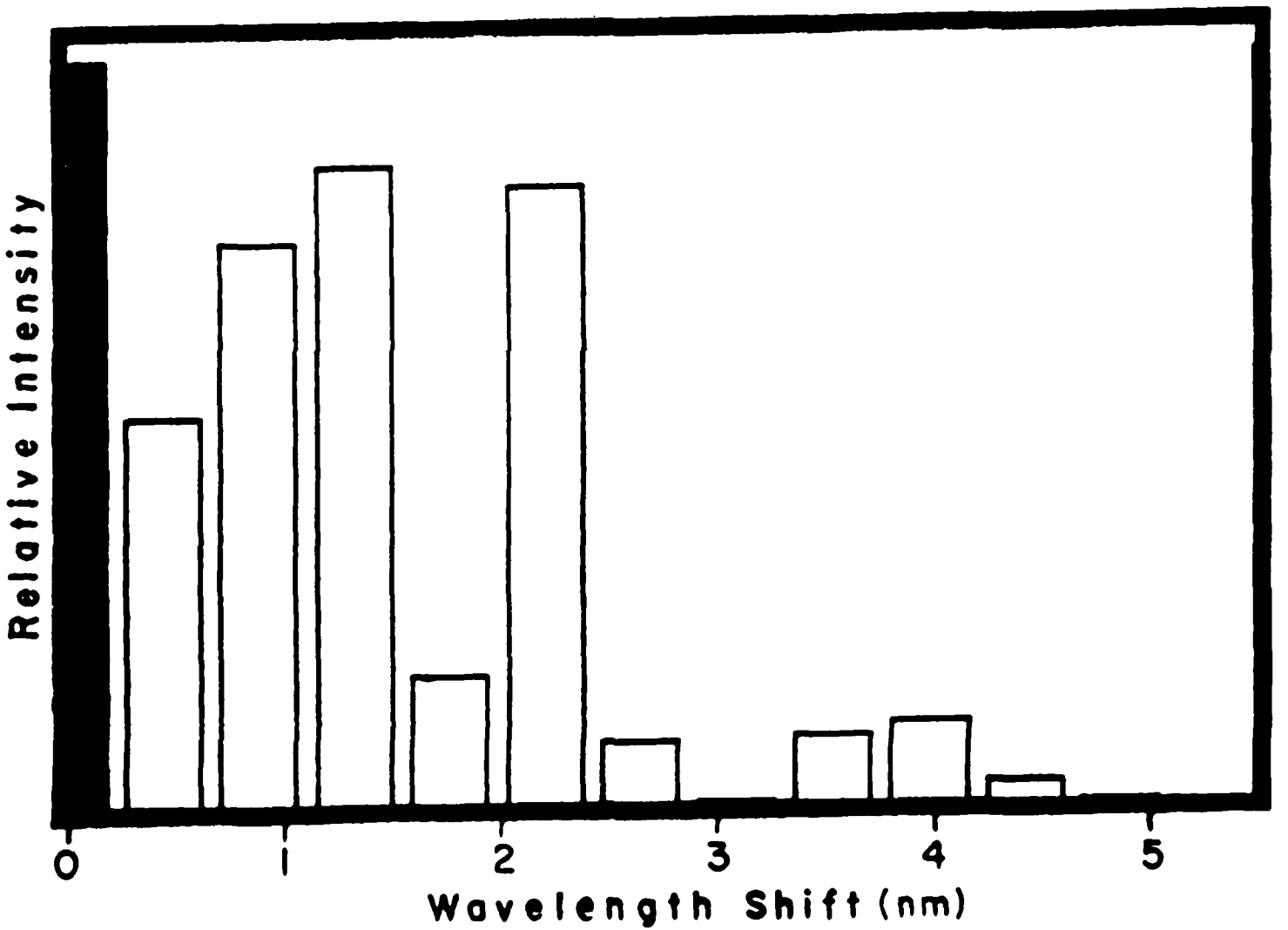

Fig. 12

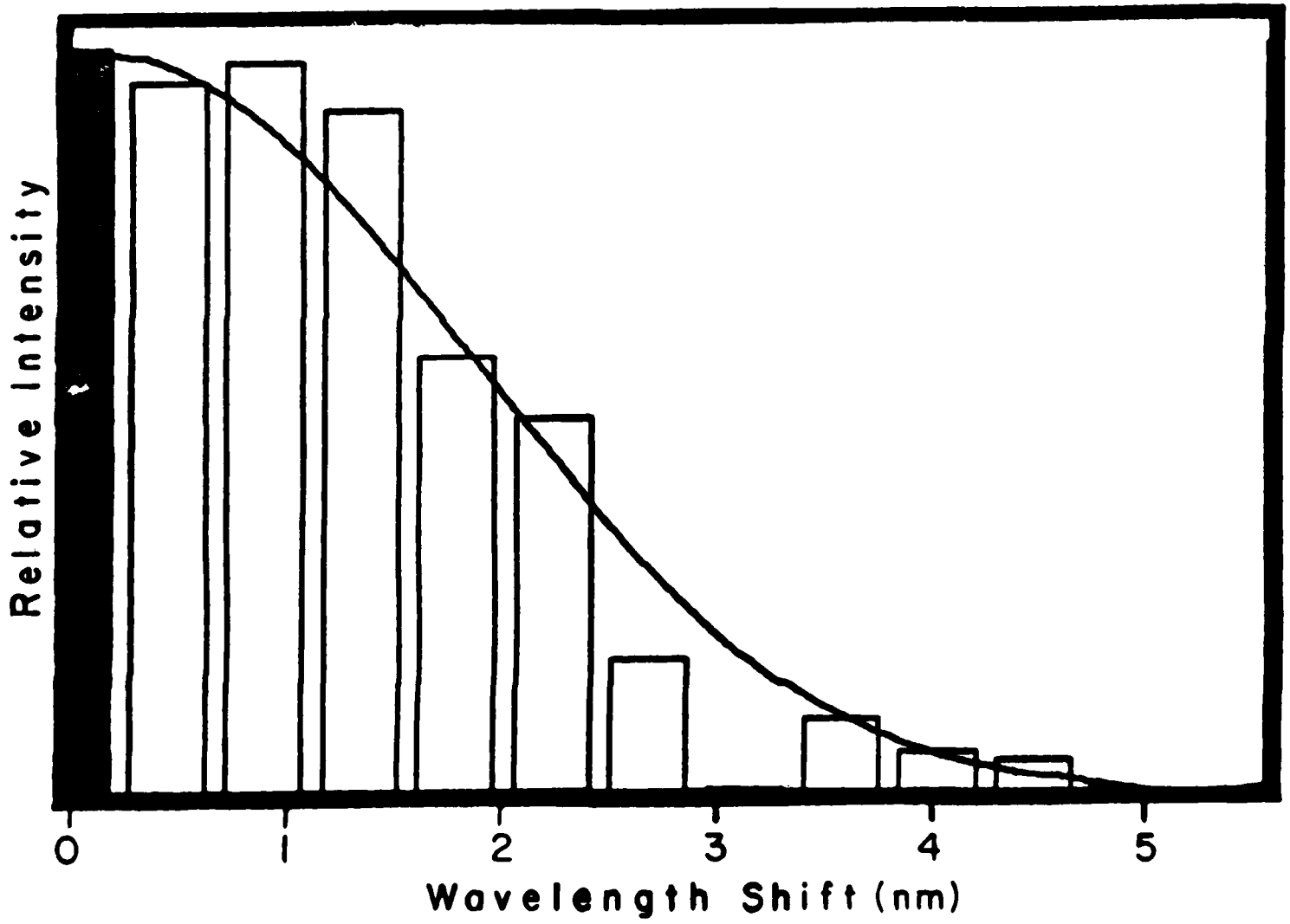

Fig. 13

TECHNICAL REPORT DISTRIBUTION LIST, GEN

	No. Copies
Office of Naval Research Attn: Code 1113 800 N. Quincy Street Arlington, Virginia 22217-5000	2
Dr. Bernard Douda Naval Weapons Support Center Code 50C Crane, Indiana 47522-5050	1
Naval Civil Engineering Laboratory Attn: Dr. R. W. Drisko, Code L52 Port Hueneme, California 93401	1
Defense Technical Information Center Building 5, Cameron Station Alexandria, Virginia 22314	12 high quality
DTNSRDC Attn: Dr. H. Singerman Applied Chemistry Division Annapolis, Maryland 21401	1
Dr. William Tolles Superintendent Chemistry Division, Code 6100 Naval Research Laboratory Washington, D.C. 20375-5000	1
Dr. David Young Code 334 NORDA NSTL, Mississippi 39529	1
Naval Weapons Center Attn: Dr. Ron Atkins Chemistry Division China Lake, California 93555	1
Scientific Advisor Commandant of the Marine Corps Code RD-1 Washington, D.C. 20380	1
U.S. Army Research Office Attn: CRD-AA-IP P.O. Box 12211 Research Triangle Park, NC 27709	1
Mr. John Boyle Materials Branch Naval Ship Engineering Center Philadelphia, Pennsylvania 19112	1
Naval Ocean Systems Center Attn: Dr. S. Yamamoto Marine Sciences Division San Diego, California 91232	1

END

DATE

FILMED

5-88

DTIC